ACS Catalysis

Research Article

pubs.acs.org/acscatalysis

Catalytic Consequences of Chemisorbed Oxygen during Methanol Oxidative Dehydrogenation on Pd Clusters

Weifeng Tu and Ya Huei (Cathy) Chin*

Department of Chemical Engineering and Applied Chemistry, University of Toronto, Toronto M5S 3E5, Ontario, Canada

Supporting Information

ABSTRACT: Surface oxygen contents and thermodynamic activities of nanosized Pd clusters and their connection to the reactivities for methanol oxidative dehydrogenation are established from rate measurements in the kinetically controlled regime and oxygen uptake studies at chemical equilibrium. First-order rate coefficients for methanol oxidative dehydrogenation (turnover rates divided by CH_3OH pressure) are single-valued functions of the oxygen-to-methanol ratio in the contacting gas phase because this ratio determines the oxygen coverages, the relative abundance of chemisorbed oxygen and unoccupied Pd sites, and in turn, the identities of the kinetically relevant steps at Pd cluster surfaces. As the oxygen-to-methanol ratio increases, the most abundant surface intermediates on Pd clusters vary from uncovered to saturated with chemisorbed oxygen; in response to this shift in coverages, the kinetically relevant step concomitantly varies from oxygen dissociation, to CH_3OH activation on oxygen adatom and oxygen vacancy pairs (O*−*), and then to CH_3OH activation on oxygen adatom pairs (O*−O*), during which the first-order rate coefficients initially increase and then reach a maximum value before decreasing to a constant value that does not vary with the oxygen-to-methanol ratio. These dependencies reflect the dual catalytic functionality of chemisorbed oxygen, first promoting the methanol conversion as the oxygen coverages increase and then inhibiting the reaction at near O* saturation, as oxygen displaces the unoccupied Pd sites, thus removing the O*−* centers while replacing them with less reactive O*−O* centers for CH_3OH activation. Methanol acts as a surface oxygen scavenger that reduces the oxygen chemical potential at Pd cluster surfaces during its catalytic turnovers. The oxygen-scavenging step by methanol increases with temperature to a larger extent than the O_2 activation step. As a result of more effective oxygen removal (by reactions) at higher temperatures, the critical oxygen coverage required for the transition of regimes from *−* to O*−* as the predominant surface sites occurs at higher oxygen-to-methanol ratios. Larger Pd clusters are more reactive for methanol oxidative dehydrogenation than smaller clusters in all regimes because cluster dimension influences the relative abundance of chemisorbed oxygen and unoccupied Pd sites, the oxygen binding strengths, and their reactivities. The direct connection of first-order rate coefficient and oxidant-to-reductant ratio appears to be general for methanol oxidative dehydrogenation on other transition metals and for oxidation catalysis, for which the reductant scavenges the chemisorbed oxygen effectively, thus dictating their coverages and thermodynamic activities.

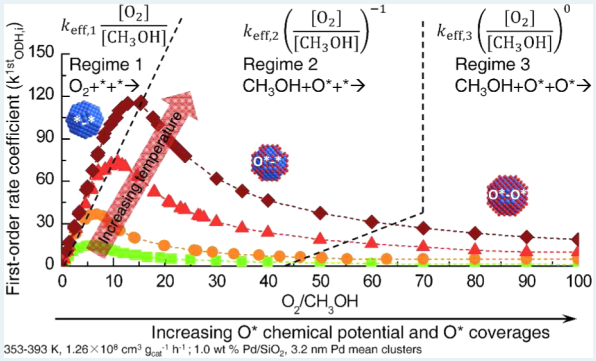

KEYWORDS: *methanol, oxidation catalysis, oxygen chemical potential, palladium, oxygen coverages, partial oxidation, oxidative dehydrogenation, kinetic regime*

1. INTRODUCTION

Light alcohols react with chemisorbed oxygen atoms on metal clusters (CH_3OH oxidation on Au,[1] Pt,[2] and Pd;[3] C_2H_5OH oxidation on Pd[3] and Au;[4−6] C_3H_7OH oxidation on Pt and Pd electrodes[7]) or with lattice oxygen on metal oxide domains (CH_3OH oxidation on V_2O_5,[8] RuO_2,[9] Fe_2O_3,[10] and MoO_3;[10] C_2H_5OH oxidation on RuO_2[9]) via kinetically coupled alcohol and oxygen activation steps at near-ambient conditions in both vapor and liquid media, forming formates, aldehydes, ketones, and esters. Vapor-phase oxidation of light alcohols (CH_3OH,[11−17] C_2H_5OH,[18] C_3H_7OH[19]) on oxygen-covered metal {Au(111),[11,12,18,19] Ag(211),[13] Cu(110),[14] Pt(211),[13] Pd(211),[13] Ir(111),[15] and Rh(211)[13]} or metal oxide {RuO_2(110)[16] and MgO(100)[17]} surfaces involves O−H bond scission of the alcohols assisted by reactive oxygen atoms. For the case of methanol, the catalytic involvement of chemisorbed oxygen atoms in methanol activation leads the first-order rate coefficients (turnover rates divided by CH_3OH pressure) to initially increase and then reach a constant value with increasing oxygen chemical potentials, as oxygen coverages on Pt, Ag, and RuO_2 cluster surfaces increase from largely uncovered to saturated with oxygen.[2,20] Here, we report a distinct dependence of first-order rate coefficients on Pd cluster surfaces for which their values initially increase, reach a

Received: January 14, 2015
Revised: April 16, 2015
Published: May 4, 2015

DOI: 10.1021/acscatal.5b00068
ACS Catal. 2015, 5, 3375−3386

transition point, and then decrease to a constant value as oxygen chemical potential increases. The bimodal kinetic dependence, undetected on other metals (i.e., Pt, RuO_2, Ag), reflects the dual catalytic roles of oxygen in promoting or inhibiting methanol catalytic turnovers on Pd clusters. The mechanistic interpretation of this unique dependency, its connection to the surface contents and thermodynamic activities of oxygen, and the catalytic functions of oxygen deserve further investigations.

We probe here the peculiar bimodal, generalized correlation of the first-order rate coefficient on operating oxygen-to-methanol ratio. We confirm that these kinetic phenomena are intrinsic catalytic events, uncorrupted by transport artifacts, by rigorous removal of temperature and concentration gradients within catalyst bed and pellets. These intrinsic rates, when combined with equilibrium oxygen uptakes, allow us to conclude that first-order rate coefficients are single-valued functions of the operating oxygen-to-methanol ratio, categorized in three distinct kinetic regimes, each with a unique kinetically relevant step and identity of most abundant reactive intermediates. We show that the ratio of oxygen-to-methanol and that of O_2 to CH_3OH activation rate constants define the thermodynamic activities of reactive oxygen and, in turn, the kinetic regimes and their transition through the kinetic coupling of methanol and oxygen activation steps. Pd cluster surfaces nearly saturated with chemisorbed oxygen contain a small amount of oxygen adatom and oxygen vacancy pairs that activate CH_3OH much more effectively than oxygen adatom pairs. These site pairs diminish, and the CH_3OH turnover rates concomitantly decrease as oxygen coverages reach saturation. The connection of oxygen reactivities to their binding strength was probed by varying the cluster size and average surface coordination. Larger Pd clusters are more reactive for methanol oxidative dehydrogenation because weakly bound oxygen atoms prevalent on these larger clusters are more effective for CH_3OH activation (in regimes 2 and 3) and contain a larger fraction of unoccupied Pd sites available for O_2 dissociation (in regime 1) than smaller clusters. As the temperature increases, higher oxygen-to-methanol ratios are required for attaining the critical oxygen coverage for the transition between regimes because smaller activation energies for O_2 than CH_3OH activation result in a decrease in rate constant ratios for O_2 to CH_3OH activation. The bimodal dependencies of rate coefficients with oxidant-to-reductant ratios, shown here for CH_3OH oxidation on Pd, appear to be general for several classes of oxidation catalytic systems (CH_4[21−23] or C_2H_6[23] oxidation on Pt) which involve oxygen vacancies as active sites and under conditions that the oxygen recombination rates are kinetically inconsequential and, as a result, the oxidant-to-reductant ratio rigorously reflects the oxygen coverages and the thermodynamic activities of oxygen at cluster surfaces.

2. EXPERIMENTAL METHODS

2.1. Synthesis and Characterizations of Supported Pd Clusters. Pd/SiO_2 (0.5 or 1.0 wt % Pd) catalysts were synthesized by incipient wetness impregnation of SiO_2 with an aqueous palladium(II) nitrate solution, prepared from dissolving the Pd salt [$Pd(NO_3)_2$, Sigma-Aldrich, 99.995% trace metals basis] in doubly deionized water. Silica (Grace, Davisil Chromatographic Silica, 330 $m^2\ g^{-1}$, 1.25 $cm^3\ g^{-1}$ pore volume, 0−75 μm particle size) was treated in ambient air by heating to 673 at 0.033 K s^{-1} and holding for 3 h before the incipient wetness impregnation step with Pd precursor solution. The impregnated sample was kept at 353 K for 24 h under ambient air and then treated in flowing dry air (Linde, 99.99%, 0.3 $cm^3\ g_{cat}^{-1}\ s^{-1}$) by increasing the temperature at 0.05 K s^{-1} to and holding isothermally at 673 K for 5 h. Portions of the Pd samples were subsequently treated under flowing dry air (Linde, 99.99%, 0.3 $cm^3\ g_{cat}^{-1}\ s^{-1}$, 0.05 K s^{-1} ramp) at temperatures between 673 and 1073 K for 5 h to vary the average Pd cluster size. These samples were cooled to ambient temperature in flowing dry air and then treated at 673 K (0.033 K s^{-1}) in 5% H_2/He (Linde certified standard to be 5.22%, 0.3 $cm^3\ g_{cat}^{-1}\ s^{-1}$) for 1 h before cooling to ambient temperature in He (Linde, 99.999%, 0.3 $cm^3\ g_{cat}^{-1}\ s^{-1}$). The samples were exposed to flowing 1% O_2/He (0.3 $cm^3\ g_{cat}^{-1}\ s^{-1}$) at ambient temperature for 6 h before exposure to ambient conditions. These catalyst powders were diluted with SiO_2 (Grace, Davisil Chromatographic Silica, 330 $m^2\ g^{-1}$ surface area, 1.25 $cm^3\ g^{-1}$ pore volume, 0−75 μm particle size) at a SiO_2-to-catalyst mass ratio of 200 and subsequently pelleted and sieved to retain 125−180 μm agglomerates.

The Pd dispersion (the fraction of Pd atoms at cluster surfaces) in these samples was determined from irreversible O_2 uptakes at 313 K between 0 and 50 kPa O_2 after the samples were treated in situ in flowing H_2 (Linde, 99.999%, 0.3 $cm^3\ g_{cat}^{-1}\ s^{-1}$) at 673 K for 1 h, exposed to dynamic vacuum (1×10^{-6} Pa to 5×10^{-2} Pa) at 673 K for 10 h, and then cooled under dynamic vacuum (1×10^{-6} Pa to 5×10^{-2} Pa) to 313 K. The average cluster diameters were estimated from these dispersion values by assuming an atomic O-to-surface Pd ratio of one ($O/Pd_s = 1$; where subscript s denotes surface Pd) and Pd clusters in hemispherical shapes with a density of bulk Pd metal (12.0 g cm^{-3}).[24] The ratio of atomic oxygen-to-total Pd atoms and the chemical state of Pd clusters were determined by isothermal volumetric oxygen uptakes at 373 K.

2.2. Steady-State Catalytic Rate and Selectivity Measurements. The Pd/SiO_2 and SiO_2 agglomerates (described in section 2.1) were physically mixed with SiO_2 (Grace, Davisil Chromatographic Silica, 330 $m^2\ g^{-1}$ surface area, 1.25 $cm^3\ g^{-1}$ pore volume, 125−180 μm particle size) to form a packed catalyst bed with an overall SiO_2-to-catalyst mass ratio of 5700 to avoid intraparticle and bed gradients in temperature or concentration. The SiO_2 did not give detectable rates under all reaction conditions reported herein ($r_{SiO_2}/r_{Pd/SiO_2} < 0.01$ when compared at the same weight of SiO_2 between 323 and 393 K). The catalyst and diluent mixtures were held on a quartz supporting frit in a tubular microcatalytic plug flow reactor (8.1 mm reactor i.d.) equipped with a K-type thermocouple placed at the center of the packed bed. All samples were treated in situ under flowing H_2 (Linde, 99.999%, 0.2×10^4−1.3×10^4 $cm^3\ g_{cat}^{-1}\ s^{-1}$) to 673 at 0.083 K s^{-1}, held for 1 h, and then cooled to reaction temperature in flowing He (Linde, 99.999%, 0.2×10^4−1.3×10^4 $cm^3\ g_{cat}^{-1}\ s^{-1}$) before exposure to CH_3OH−O_2 reactants. Reactant mixtures were prepared from either 5.5% O_2/He (Linde certified standard) or pure O_2 (Linde, 99.995%), CH_3OH (Sigma-Aldrich, anhydrous, 99.8%), and He (Linde, 99.999%). Gas flow rates of 5.5% O_2/He, pure O_2, and He were independently metered using electronic mass flow controllers to achieve a space velocity between 1.5×10^7 and 2.5×10^8 $cm^3\ g_{cat}^{-1}\ h^{-1}$. Liquid methanol was introduced using a gastight syringe (Hamilton, 5 cm^3) mounted on a syringe infusion pump (KD Scientific, LEGATO 100) at a constant infusion rate (0.055−0.280 $cm^3\ h^{-1}$) into a heated zone maintained at 338 K, in which it was

DOI: 10.1021/acscatal.5b00068
ACS Catal. 2015, 5, 3375−3386

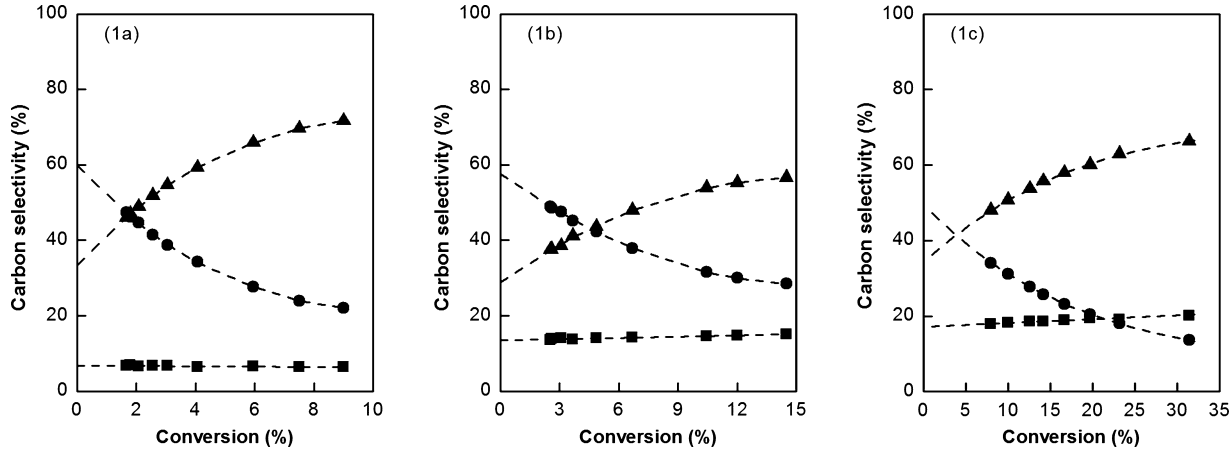

Figure 1. Carbon selectivities (CO_2 (■), HCHO (●), and $HCOOCH_3$ (▲)) during CH_3OH-O_2 reactions at 373 K on 1.0 wt % Pd/SiO_2 catalyst (3.2 nm mean Pd cluster diameter) as a function of methanol conversion with O_2/CH_3OH feed mixtures of 1.5 (a), 9 (b), and 60 (c) (200 SiO_2-to-catalyst intraparticle and 5700 SiO_2-to-catalyst interparticle dilution ratios; 1.5×10^7-2.5×10^8 cm^3 g_{cat}^{-1} h^{-1}).

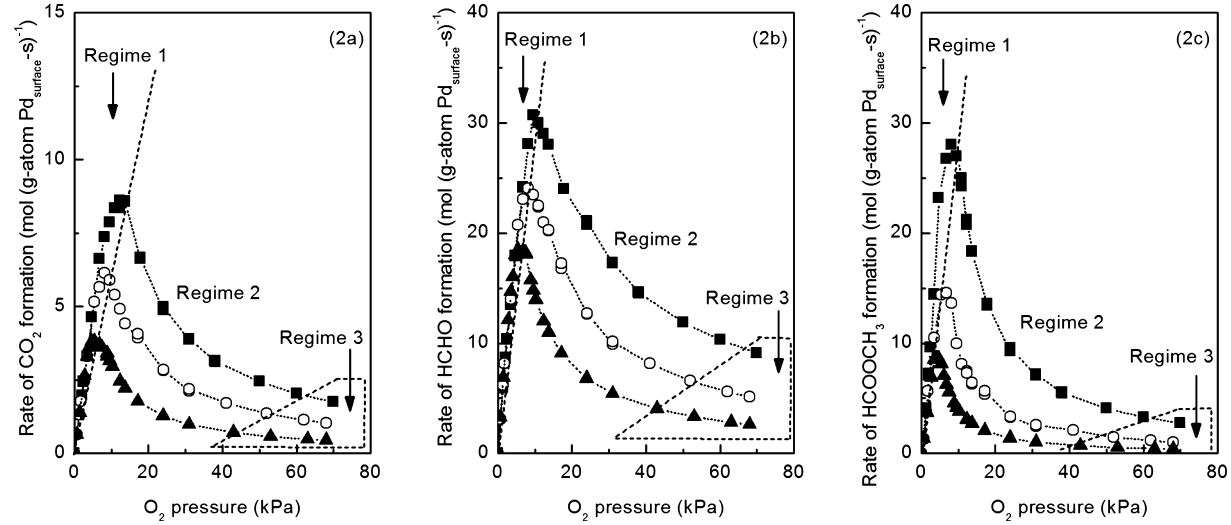

Figure 2. Turnover rates for CO_2 ($r_{CO_2,i}$, a), HCHO ($r_{HCHO,i}$, b), and $HCOOCH_3$ ($r_{HCOOCH_3,i}$, c) formation as a function of O_2 pressure during CH_3OH-O_2 reactions (0.75 kPa (▲), 1.25 kPa (○), and 1.75 kPa (■) CH_3OH) on 1.0 wt % Pd/SiO_2 at 373 K (3.2 nm mean Pd cluster diameter, 200 SiO_2-to-catalyst intraparticle and 5700 SiO_2-to-catalyst interparticle dilution ratios; 1.26×10^8 cm^3 g_{cat}^{-1} h^{-1}; subscript i in $r_{CO_2,i}$, $r_{HCHO,i}$, and $r_{HCOOCH_3,i}$ denotes regime i (i = 1, 2, or 3); kinetic regimes 1, 2, and 3 are labeled as regimes 1, 2, and 3, respectively, in the figure).

evaporated and mixed with the gas feed stream containing O_2 and He. All transfer gas lines were heated to 373 K to prevent condensation of reactants and products. The chemical compositions of the reactant and product streams were quantified using a micro gas chromatograph (Varian CP-4900) equipped with HP-PLOT U (CP 4900 backflush column module, 10 m) and Molecular Sieve 5A (CP 4900 backflush column module, 10 m) columns connected to thermal conductivity detectors. Rates of CO_2, HCHO, and $HCOOCH_3$ formation and methanol oxidative dehydrogenation at various CH_3OH and O_2 pressures were measured in the kinetically controlled regime, attained by keeping the reactor heat load below 0.023 W s^{-1}, as demonstrated elsewhere,[2] and at methanol and oxygen conversions below 10%, taken after reaching steady state, during which the changes in rates were less than 5% of their values, measured at a reference condition (O_2-to-CH_3OH = 1.5, space velocity of 1.26×10^8 cm^3 g_{cat}^{-1} h^{-1}) for the entire duration of rate measurements (~20 h).

3. RESULTS AND DISCUSSION

3.1. Selectivities and Reaction Network for Methanol Partial Oxidation on Pd Clusters. The selectivity of carbon-containing products (species j, j = CO_2, HCHO, and $HCOOCH_3$) is defined as the molar flow rate ratio of CH_3OH converted into species j to CH_3OH reacted. As an example, the selectivity toward $HCOOCH_3$ is determined from the molar flow rate of CH_3OH converted to $HCOOCH_3$ (which also equals twice of the molar flow rate of $HCOOCH_3$ in the reactor effluent) over the total molar flow rate of CH_3OH reacted (determined by subtracting the molar flow rate of CH_3OH at the effluent stream from the molar flow rate of CH_3OH in the feed) because each $HCOOCH_3$ is formed from two CH_3OH molecules. Parts a–c of Figure 1 show the selectivities of carbon-containing products (CO_2, HCHO, and $HCOOCH_3$) for CH_3OH-O_2 reactions as a function of CH_3OH conversion, obtained by varying the residence time, for three O_2-to-CH_3OH feed ratios of 1.5, 9, and 60 on Pd clusters (1.0 wt % Pd/SiO_2, 3.2 nm Pd cluster diameter) at 373 K. CO,

DOI: 10.1021/acscatal.5b00068
ACS Catal. 2015, 5, 3375–3386

HCOOH, and H_2 were undetected (<5 ppmv, which correspond to CO, HCOOH, and H_2 selectivities of less than 0.4%, 0.4%, and 0.1%, respectively) over the entire range of O_2-to-CH_3OH ratios (0.1−100; 0.5−5 kPa CH_3OH and 0.1−70 kPa O_2) at 373 K, consistent with previously reported selectivites for Pd catalysts;[3,25] similar products were also found on dispersed Pt clusters.[2,26] Carbon selectivities toward HCHO decreased and those for $HCOOCH_3$ and CO_2 concomitantly increased as the CH_3OH conversion and residence time increased for all O_2-to-CH_3OH ratios (1.5, 9, and 60, Figure 1). Extrapolation of these selectivity values to zero conversion minimizes the rate contributions from secondary reactions; these selectivities reflect the relative rates of CO_2, HCHO, and $HCOOCH_3$ formation predominantly from primary reactions. The nonzero selectivity values (6.8% CO_2, 59.9% HCHO, and 33.1% $HCOOCH_3$ for O_2/CH_3OH = 1.5; 13.5% CO_2, 57.4% HCHO, and 29.1% $HCOOCH_3$ for O_2/CH_3OH = 9; 17.1% CO_2, 49.4% HCHO, and 34.3% $HCOOCH_3$ for O_2/CH_3OH = 60), which we interpret as indicative that all three products (CO_2, HCHO, and $HCOOCH_3$) can form directly from primary reactions between methanol and oxygen derived species on Pd cluster surfaces. $HCOOCH_3$−O_2 reactions at similar space velocities did not lead to CO_2, HCHO, or CH_3OH at detectable values on Pd (313 K, 45 kPa O_2 and 0.3 kPa $HCOOCH_3$ feed),[3] as also found on Pt (373−450 K, 0.1−40 kPa O_2, and 0.6 kPa $HCOOCH_3$ feed).[2] These findings led us to conclude that all carbon containing products may be formed directly from CH_3OH and portions of CO_2 and $HCOOCH_3$ are formed from HCHO oxidation and HCHO acetalization with methanol derived surface intermediates, respectively, as found previously on Pt/SiO_2 (373 K),[2] Pd/γ-Al_2O_3 (313 K),[3] and Au nanofibers between 10 and 50 nm (293−353 K).[1]

Figure 2 shows the turnover rates [unit: mol (g-atom $Pd_{surface}$-s)$^{-1}$, defined as the mole of product (CO_2, HCHO, or $HCOOCH_3$) formed per mole of surface Pd atom per time] for CO_2 (Figure 2a), HCHO (Figure 2b), and $HCOOCH_3$ (Figure 2c) formation at various CH_3OH pressures (0.5−2.0 kPa), plotted against the O_2 pressure over a wide range of O_2-to-CH_3OH ratios (0.1−100) on Pd clusters (1.0 wt % Pd/SiO_2, 3.2 nm mean Pd cluster diameter) at 373 K. Turnover rates for CO_2, HCHO, and $HCOOCH_3$ formation vary with O_2 and CH_3OH pressures differently depending on the range of O_2-to-CH_3OH ratio. These variations in rate dependencies are categorized here in three kinetic regimes (regime 1: 0.1−7 O_2/CH_3OH, regime 2: 7−50 O_2/CH_3OH, regime 3: 50−100 O_2/CH_3OH) based on the operating O_2-to-CH_3OH ratio, as highlighted in Figure 2. The rate of formation for carbon species j (j = HCHO, $HCOOCH_3$, or CO_2) per surface Pd atom in regime i (i = 1, 2, or 3) is denoted as $r_{j,i}$ and expressed in a general form (eq 1) that varies with the CH_3OH and O_2 pressures (denoted as $[CH_3OH]$ and $[O_2]$, respectively)

$$r_{j,i} = k_{app,j,i}[CH_3OH]^{\alpha_{j,i}}[O_2]^{\beta_{j,i}} \quad (1)$$

where $k_{app,j,i}$ is the apparent rate constant for species j in regime i and $\alpha_{j,i}$ and $\beta_{j,i}$ are the apparent reaction orders with respect to CH_3OH and O_2, respectively, for species j in regime i.

At low O_2-to-CH_3OH ratios (<7, regime 1), turnover rates for CO_2 formation increased linearly with O_2 ($\beta_{CO_2,1}$ = 1.0 ± 0.1), whereas those for HCHO formation increased less than linearly ($\beta_{HCHO,1}$ = 0.8 ± 0.1) and for $HCOOCH_3$ formation increased more than linearly ($\beta_{HCOOCH_3,1}$ = 1.3 ± 0.1) with O_2. The turnover rates for CO_2 formation did not vary with CH_3OH pressure ($\alpha_{CO_2,1}$ = 0.0 ± 0.1) and for HCHO and $HCOCCH_3$ formation varied weakly with CH_3OH pressure ($\alpha_{HCHO,1}$ = −0.1 ± 0.1 and $\alpha_{HCOOCH_3,1}$ = 0.3 ± 0.1). As the O_2-to-CH_3OH ratio increased to above 7 and below 50 (regime 2), the rates of CO_2, HCHO, and $HCOOCH_3$ formation began to acquire a negative dependence with O_2 pressure ($\beta_{CO_2,2}$ = −1.0 ± 0.1, $\beta_{HCHO,2}$ = −0.8 ± 0.1, and $\beta_{HCOOCH_3,2}$ = −1.2 ± 0.1) and depended more than linearly and much more strongly on CH_3OH pressure ($\alpha_{CO_2,2}$ = 1.7 ± 0.2, $\alpha_{HCHO,2}$ = 1.3 ± 0.3, and $\alpha_{HCOOCH_3,2}$ = 2.4 ± 0.3) than in regime 1. A further increase in O_2-to-CH_3OH ratio to above 50 (regime 3) led all product formation rates to become independent of O_2 pressure ($\beta_{CO_2,3}$ = $\beta_{HCHO,3}$ = $\beta_{HCOOCH_3,3}$ = 0.0 ± 0.1) and depend less strongly on CH_3OH pressure ($\alpha_{CO_2,3}$ = 0.8 ± 0.2, $\alpha_{HCHO,3}$ = 0.5 ± 0.2, and $\alpha_{HCOOCH_3,3}$ = 1.7 ± 0.2) than in regime 2. These transitions in rate dependence in response to changing O_2-to-CH_3OH ratio appear to reflect a direct connection of the operating O_2-to-CH_3OH ratio to the nature and relative abundances of the surface intermediates and the prevalent kinetically relevant steps during methanol oxidation catalysis. Next, we focus on interpreting the rates of methanol oxidative dehydrogenation, as these rates reflect the effective collisional frequencies for the initial methanol activation during their catalytic sojourns on Pd clusters without the contributions from methanol molecules consumed by secondary reactions.

3.2. First-Order Rate Coefficients for Methanol Oxidative Dehydrogenation Are Single-Valued Functions of O_2-to-CH_3OH Ratio. Turnover rates for CH_3OH oxidative dehydrogenation (ODH), $r_{ODH,i}$ (subscript "ODH,i" refers to oxidative dehydrogenation reaction in regime i), were reported as the combined rates for HCHO, CO_2, and $HCOOCH_3$ formation ($r_{ODH,i} = r_{CO_2,i} + r_{HCHO,i} + r_{HCOOCH_3,i}$)[9] because HCHO, CO_2, or $HCOOCH_3$ formation each requires a catalytic CH_3OH sojourn. The turnover rates [$r_{ODH,i}$, mol (g-atom $Pd_{surface}$-s)$^{-1}$; mole of CH_3OH per mole of surface Pd atom per time] divided by CH_3OH pressure ($[CH_3OH]$) give the first-order rate coefficients [$k^{1st}_{ODH,i}$, mol (g-atom $Pd_{surface}$-s-kPa)$^{-1}$] for oxidative dehydrogenation reaction:

$$k^{1st}_{ODH,i} = \frac{r_{ODH,i}}{[CH_3OH]} \quad (2)$$

Their values for CH_3OH−O_2 reactions on Pd clusters (1.0 wt % Pd/SiO_2, 3.2 nm mean Pd cluster diameter, 373 K) are single-valued functions of the operating O_2-to-CH_3OH ratios, as shown in Figure 3, irrespective of individual CH_3OH and O_2 pressures. O_2-to-CH_3OH values dictate the kinetic dependencies and their transition; thus, they define the operating boundaries for regimes 1−3 (regime 1: 0.1−7 O_2/CH_3OH, regime 2: 7−50 O_2/CH_3OH, and regime 3: 50−100 O_2/CH_3OH). The single-valued functional dependence of first-order rate coefficients on O_2-to-CH_3OH ratios was also found for Pt, Ag, and RuO_2 clusters: the rate coefficients were found to either increase or remain unchanged with the O_2-to-CH_3OH ratio at the two operating regimes corresponded to regimes 1 and 3, respectively.[20] The regime corresponded to the intermediate O_2-to-CH_3OH ratios (regime 2) was, however, not being detected on these clusters.

DOI: 10.1021/acscatal.5b00068
ACS Catal. 2015, 5, 3375−3386

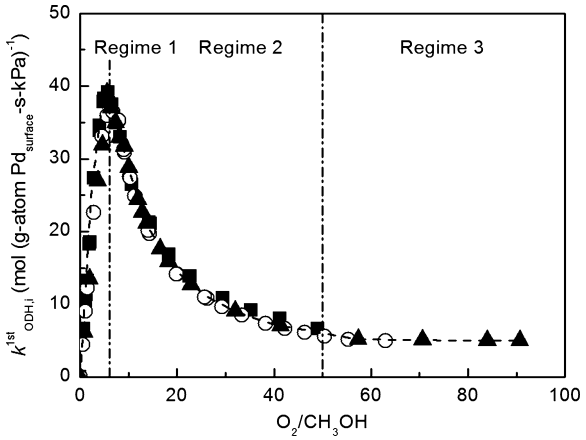

Figure 3. First-order rate coefficients ($k^{1st}_{ODH,i}$=$r_{ODH,i}$ $[CH_3OH]^{-1}$, subscript i denotes regime i (i = 1, 2, or 3)) for CH_3OH oxidative dehydrogenation (ODH) as single-valued functions of O_2-to-CH_3OH ratio during CH_3OH–O_2 reactions (0.75 kPa (▲), 1.25 kPa (○), and 1.75 kPa (■) CH_3OH) at 373 K on 1.0 wt % Pd/SiO_2 (3.2 nm mean Pd cluster diameter, 200 SiO_2-to-catalyst intraparticle and 5700 SiO_2-to-catalyst interparticle dilution ratios; 1.26×10^8 cm^3 g_{cat}^{-1} h^{-1}; kinetic regimes 1, 2, and 3 are labeled as regimes 1, 2, and 3, respectively, in the figure).

In regime 1 ($0.1 < O_2/CH_3OH < 7$), first-order rate coefficients ($k^{1st}_{ODH,1}$) increased proportionally with O_2-to-CH_3OH ratios (Figure 3)

$$k^{1st}_{ODH,1} = \frac{r_{ODH,1}}{[CH_3OH]} = k_{eff,1}\left(\frac{[O_2]}{[CH_3OH]}\right) \quad (3)$$

where $k_{eff,1}$ denotes the effective rate constant for CH_3OH oxidative dehydrogenation in regime 1. CH_3OH turnover rates in this regime vary linearly with O_2 pressure ($\beta_{ODH,1}$ = 1.0 ± 0.1, Table 1) and are insensitive to CH_3OH pressure ($\alpha_{ODH,1}$ = 0.0 ± 0.1, Table 1), consistent with rates limited by oxygen activation on Pd cluster surfaces largely uncovered of reactive intermediates[2] (derivation in section S1 in Supporting Information)

$$r_{ODH,1} = k_{O_2,f}[O_2] \quad (4)$$

where $k_{O_2,f}$ denotes the rate constant for oxygen dissociation on Pd clusters. The measured rate constant for oxygen dissociation on Pd clusters free of reactive intermediates, $k_{O_2,f}$, is 6.7 ± 0.5 mol O_2 (g-atom $Pd_{surface}$-s-kPa)$^{-1}$ at 373 K, obtained from linear regression of rate data in regime 1 from Figure 3 with eq 4.

As the O_2-to-CH_3OH ratio increased to above 7 but below 50, the transition from regime 1 to regime 2 occurred, during which the first-order rate coefficients ($k^{1st}_{ODH,2}$) varied inversely with O_2-to-CH_3OH ratio (Figure 3)

$$k^{1st}_{ODH,2} = \frac{r_{ODH,2}}{[CH_3OH]} = k_{eff,2}\left(\frac{[O_2]}{[CH_3OH]}\right)^{-1} \quad (5)$$

where $k_{eff,2}$ denotes the effective rate constant for methanol oxidative dehydrogenation in regime 2. The linear relation between the first-order rate coefficients ($k^{1st}_{ODH,2}$) and the inverse of O_2-to-CH_3OH ratio $[([O_2]/[CH_3OH])^{-1}]$ is confirmed in Figure 4, and the regression of these data against

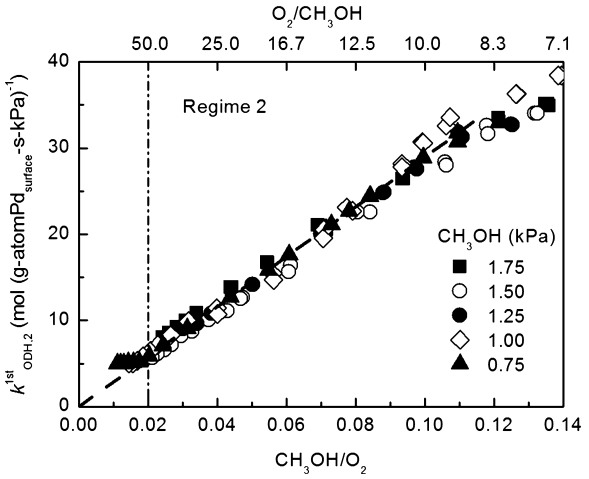

Figure 4. First-order rate coefficients ($k^{1st}_{ODH,2}$ = $r_{ODH,2}$ $[CH_3OH]^{-1}$) for CH_3OH oxidative dehydrogenation (ODH) in regime 2 on 1.0 wt % Pd/SiO_2 (3.2 nm mean Pd cluster diameter) at 373 K as a function of CH_3OH-to-O_2 ratio (O_2/CH_3OH = 7–50; 200 SiO_2-to-catalyst intraparticle and 5700 SiO_2-to-catalyst interparticle dilution ratios; 1.26×10^8 cm^3 g_{cat}^{-1} h^{-1}).

eq 5 gives $k_{eff,2}$ of 290 ± 10 mol (g-atom $Pd_{surface}$-s-kPa)$^{-1}$ at 373 K. This relation of $k^{1st}_{ODH,2}$ and the inverse of O_2-to-CH_3OH ratio (eq 5) arises from a second-order dependence of rates on CH_3OH and an inverse dependence of rates on O_2, as shown in section S2 of the Supporting Information, Figures S1a

Table 1. Observed Rate Dependencies and Apparent Reaction Orders for CH_3OH Oxidative Dehydrogenation (ODH) and for HCHO, CO_2, and $HCOOCH_3$ Formation, Identity of the Most Abundant Surface Intermediates (MASI), and the Active Sites during CH_3OH–O_2 Reactions on 1.0 wt % Pd/SiO_2 in Kinetic Regimes 1–3 at 373 K[a]

kinetic regime i	regime 1 ($0.1 < O_2/CH_3OH < 7$)	regime 2 ($7 < O_2/CH_3OH < 50$)	regime 3 ($50 < O_2/CH_3OH < 100$)
MASI	[*]	[O*]	[O*]
active sites	*–*	O*–*	O*–O*
$r_{j,i}$	$k_{app,j,1}[CH_3OH]^{\alpha}{}_{j,1}[O_2]^{\beta}{}_{j,1}$	$k_{app,j,2}[CH_3OH]^{\alpha}{}_{j,2}[O_2]^{\beta}{}_{j,2}$	$k_{app,j,3}[CH_3OH]^{\alpha}{}_{j,3}[O_2]^{\beta}{}_{j,3}$
$r_{ODH,i}$	$k_{eff,1}[CH_3OH]^0[O_2]^1$	$k_{eff,2}[CH_3OH]^2[O_2]^{-1}$	$k_{eff,3}[CH_3OH]^1[O_2]^0$
$r_{CO_2,i}$	$k_{app,CO_2,1}[CH_3OH]^0[O_2]^1$	$k_{app,CO_2,2}[CH_3OH]^{1.7}[O_2]^{-1}$	$k_{app,CO_2,3}[CH_3OH]^{0.8}[O_2]^0$
$r_{HCHO,i}$	$k_{app,HCHO,1}[CH_3OH]^{-0.1}[O_2]^{0.8}$	$k_{app,HCHO,2}[CH_3OH]^{1.3}[O_2]^{-0.8}$	$k_{app,HCHO,3}[CH_3OH]^{0.5}[O_2]^0$
$r_{HCOOCH_3,i}$	$k_{app,HCOOCH_3,1}[CH_3OH]^{0.3}[O_2]^{1.3}$	$k_{app,HCOOCH_3,2}[CH_3OH]^{2.4}[O_2]^{-1.2}$	$k_{app,HCOOCH_3,3}[CH_3OH]^{1.7}[O_2]^0$

[a] 1.26×10^8 cm^3 g_{cat}^{-1} h^{-1}, 3.2 nm mean Pd cluster diameter, 200 SiO_2-to-catalyst intraparticle and 5700 SiO_2-to-catalyst interparticle dilution ratios; the subscripts j, i in rates ($r_{j,i}$, mol (g-atom $Pd_{surface}$-s)$^{-1}$), apparent rate constants ($k_{eff,j,i}$, mol (g-atom $Pd_{surface}$-s-kPa)$^{-1}$), and apparent reaction orders ($\alpha_{j,i}$ and $\beta_{j,i}$) denote carbon-containing products j (j = CO_2, HCHO, or $HCOOCH_3$) and kinetic regime i (i = 1, 2, or 3); $k_{eff,i}$ denotes the effective rate constant for methanol oxidative dehydrogenation in regime i (i = 1, 2, or 3).

DOI: 10.1021/acscatal.5b00068
ACS Catal. 2015, 5, 3375–3386

and S1b, respectively. These rate data are consistent with kinetically relevant CH_3OH activation on oxygen adatom and oxygen vacancy pairs (O*−*) found on Pd cluster surfaces nearly saturated with chemisorbed oxygen atoms (O*), on which the relative abundances of oxygen and oxygen vacancies are given by the kinetic coupling of irreversible O_2 and CH_3OH activation steps (see derivation in section S2 of the Supporting Information)

$$r_{ODH,2} = \frac{(k_{[O^*-*]})^2}{k_{O_2,f}} \frac{[CH_3OH]^2}{[O_2]} = k_{eff,2} \frac{[CH_3OH]^2}{[O_2]} \quad (6)$$

where $k_{[O^*-*]}$ denotes the rate constant for methanol activation on an O*−* site pair at Pd cluster surfaces. The opposite assumption of quasi-equilibrated oxygen activation would instead lead the first-order rate coefficients ($k^{1st}_{ODH,2}$) to vary proportionally with $[O_2]^{-0.5}$, as the rate $r_{ODH,2}$ varies linearly with CH_3OH and inversely with O_2 to the negative one-half order, inconsistent with the observed dependencies (Figure S1a,b, Supporting Information). The $k_{[O^*-*]}$ is 44 ± 1 mol (g-atom $Pd_{surface}$-s-kPa)$^{-1}$ at 373 K, determined by nonlinear regression of the rate data in Figure 4 and assuming a constant $k_{O_2,f}$ value of 6.7 ± 0.5 mol O_2 (g-atom $Pd_{surface}$-s-kPa)$^{-1}$ throughout regimes 1 and 2. The oxygen adatom and oxygen vacancy pair (O*−*) acts as an acid−base site pair that polarizes the O−H bond of CH_3OH, by concomitant interactions of oxygen vacancy (exposed Pd, *) and CH_3O and of O* with the leaving H at the CH_3OH activation transition state; these oxygen adatom and oxygen vacancy pairs are found on metal surfaces, as previously reported for the case of O*-covered Ag(110),[27] Pt(111),[28] Pt(100),[29] and Au(111)[11] single crystal surfaces and similar lattice oxygen−metal ion pairs ($O_{ox}-M_{ox}$) on oxide surfaces of MgO(100)[17] and RuO_2(110).[16] These site pairs are also active in cleaving the O−H bond in larger alcohols [C_2H_5OH[18] and C_3H_7OH[19] on O*-covered Au(111) surfaces, and Ar−CH_2−OH (benzyl alcohol) on Pd clusters[30]] and the C−H bond in CH_3OCH_3 (on O* covered Pt clusters),[31] in CH_4 (on O* covered Pt clusters[22] and Pd(111) surfaces[32]), and in C_2H_6 (on O* covered Pt clusters)[23] via mechanistically similar pathways.

First-order rate coefficients decreased as the O_2-to-CH_3OH ratio increased because site occupation by O* led to less effective CH_3OH activation. The rate coefficients decreased to a constant value [5 ± 0.5 mol (g-atom $Pd_{surface}$-s-kPa)$^{-1}$, 373 K] for O_2-to-CH_3OH ratios above 50, which corresponds to regime 3

$$k^{1st}_{ODH,3} = \frac{r_{ODH,3}}{[CH_3OH]} = k_{eff,3}\left(\frac{[O_2]}{[CH_3OH]}\right)^0 \quad (7)$$

where $k_{eff,3}$ denotes the effective rate constant for methanol oxidative dehydrogenation in this regime. The rates increase proportionally with CH_3OH pressure ($\alpha_{ODH,3}$ = 1.0 ± 0.1, Table 1) but remain insensitive to O_2 pressure ($\beta_{ODH,3}$ = 0.0 ± 0.1, Table 1), an indication that the CH_3OH activation must be kinetically relevant and occur on Pd surfaces saturated with O*:

$$r_{ODH,3} = k_{[O^*-O^*]}[CH_3OH]^1[O_2]^0 \quad (8)$$

Here, $k_{[O^*-O^*]}$ reflects the elementary rate constant of CH_3OH activation assisted by an oxygen adatom pair (O*−O*) and equals $k_{eff,3}$ in eq 7 (derivation in section S3 in the Supporting Information).

These elementary reaction steps for O_2 dissociation on *−* site pairs and CH_3OH activation on O*−* and O*−O* site pairs occur concurrently in all regimes, but their relative contributions to the observed rates differ markedly because of the difference in site abundances of chemisorbed oxygen and unoccupied Pd sites and the extent of their participation in catalysis from one regime to another. The kinetic dependencies and the associated rate derivations were obtained for each regime when the proposed kinetically relevant step for the individual regime remains as the predominant step for CH_3OH turnovers. During the transition from one regime to another, CH_3OH turnovers contain the rate contribution from the kinetically relevant steps for both regimes and as O* coverages vary, the elementary rate and equilibrium constants for these steps may deviate from their constant values, because O* reactivities depend on O* coverages, as the coverages influence the lateral repulsive interactions between O* atoms, heats of O* adsorption, and in turn their reactivities.

3.3. Effects of Methanol Pressure on the O* Chemical Potential at Pd Cluster Surfaces. Equilibrium oxygen coverages at Pd cluster surfaces (1.0 wt % Pd/SiO_2, 3.2 nm mean Pd cluster diameter) were measured as a function of oxygen pressure (0−50 kPa O_2, without CH_3OH) at 373 K. The atomic ratios of oxygen-to-surface Pd (O/Pd_s, where subscript *s* denotes surface Pd) at equilibrium are shown in Figure 5 as a function of O_2 pressure. The O/Pd_s ratios

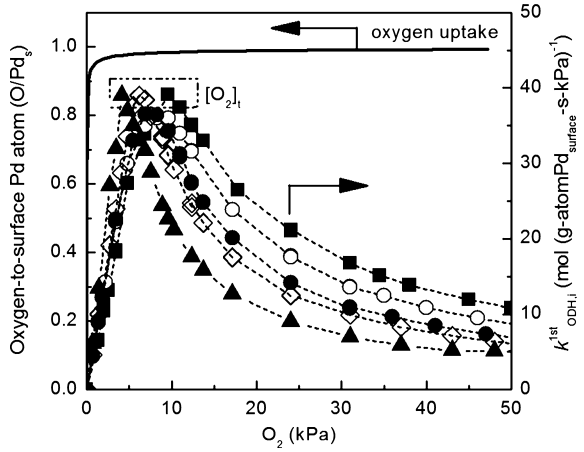

Figure 5. Atomic ratio of oxygen-to-surface Pd atom (O/Pd_s, subscript *s* denotes surface Pd) during volumetric oxygen uptakes (without CH_3OH, 373 K) and the first-order rate coefficients ($k^{1st}_{ODH,i}$ = $r_{ODH,i}[CH_3OH]^{-1}$, subscript *i* denotes regime *i* (*i* = 1, 2, or 3), 373 K) for CH_3OH oxidative dehydrogenation (ODH) on Pd clusters at 0.75 kPa (▲), 1.00 kPa (◇), 1.25 kPa (●), 1.50 kPa (○), and 1.75 kPa (■) CH_3OH, plotted against oxygen pressure. The O_2 pressure required for kinetic transition between regimes 1 and 2 is labeled in the figure as $[O_2]_t$ (1.0 wt % Pd/SiO_2, 3.2 nm mean Pd cluster diameter, 200 SiO_2-to-catalyst intraparticle and 5700 SiO_2-to-catalyst interparticle dilution ratios; 1.26 × 10^8 cm^3 g_{cat}^{-1} h^{-1}).

increased sharply (from 0.0 to 0.9) over a narrow range of O_2 pressure (0−0.25 kPa) but more gradually and then approached near unity (O/Pd_s = 0.95) at higher O_2 pressures (>1 kPa). These O/Pd_s ratios depend on the equilibrium constant for O_2 dissociative adsorption [K_{O_2}, which equals the rate constant ratio of O_2 dissociation ($k_{O_2,f}$) to O* recombination ($k_{O_2,r}$)] and oxygen pressure ([O_2]) via the following relation on Langmuirian surfaces:

DOI: 10.1021/acscatal.5b00068
ACS Catal. 2015, 5, 3375−3386

$$\frac{O}{Pd_s} = \frac{[O^*]}{[L]} = \frac{(K_{O_2}[O_2])^{0.5}}{1 + (K_{O_2}[O_2])^{0.5}} \quad (9)$$

[O*] and [L] denote the concentration of O* and total available adsorption site, respectively, on Pd cluster surfaces. The equilibrium constant for O_2 dissociation (K_{O_2}) is estimated to be 400 ± 50 kPa^{-1} at 373 K, which corresponds to the heat of oxygen dissociative adsorption of −111 kJ $(mol\ O_2)^{-1}$, by assuming complete entropy losses of O_2 of 211 J $(mol\ O_2\ K)^{-1}$ for the formation of immobile chemisorbed oxygen atoms.[33] Similar heats of oxygen dissociative adsorption (−100 ± 7 kJ mol^{-1}) are also observed on 0.5 ML oxygen covered Pd(111) surfaces in direct calorimetric measurements.[34,35]

O* coverages during steady-state methanol oxidative dehydrogenation must either be identical to or lower than those at equilibrium (without CH_3OH) because their values are given not only by the O_2 dissociation-recombination step but also by an additional pathway of O* removal from cluster surfaces via their reactions with CH_3OH. Pseudo-steady-state assumption of chemisorbed oxygen atoms leads to an equation containing the rates of O_2 dissociation ($r_{O_2,f}$), O* recombination ($r_{O_2,r}$), and O* removal via their involvement as oxygen adatom and oxygen vacancy or oxygen adatom site pairs in CH_3OH activation ($r_{CH_3OH,[O^*-*]}$ or $r_{CH_3OH,[O^*-O^*]}$):

$$\frac{dO^*}{dt} = 0 = 2r_{O_2,f} - 2r_{O_2,r} - \nu_{[O^*-*]}r_{CH_3OH,[O*-*]} - \nu_{[O^*-O^*]}r_{CH_3OH,[O*-O*]} \quad (10a)$$

$$\frac{dO^*}{dt} = 0 = 2k_{O_2,f}[O_2][*]^2 - 2k_{O_2,r}[O^*]^2 - \nu_{[O^*-*]}k_{[O^*-*]}[CH_3OH][O^*][*] - \nu_{[O^*-O^*]}k_{[O^*-O^*]}[CH_3OH][O^*]^2 \quad (10b)$$

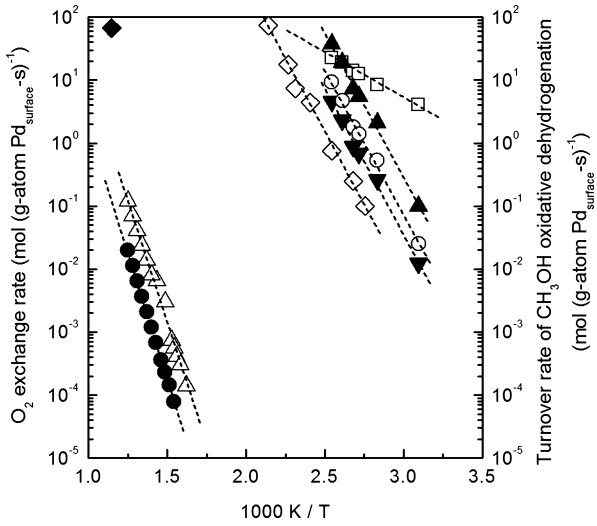

Figure 6. $^{16}O^{18}O$ isotopologue formation rates in $^{16}O_2$−$^{18}O_2$ mixtures (2 kPa O_2; 2 nm (●),[36] 8 nm (△),[36] and 21.3 nm (♦)[37] Pd clusters) and turnover rates of CH_3OH oxidative dehydrogenation in regime 1 (□; 2 kPa O_2, 0.50 kPa CH_3OH), regime 2 (2 kPa O_2; 0.07 kPa (▼), 0.10 kPa (○), and 0.20 (▲) kPa CH_3OH), and regime 3 (◊; 2 kPa O_2, 0.05 kPa CH_3OH) on Pd clusters (1.0 wt % Pd/SiO_2, 3.2 nm mean Pd cluster diameter).

Two O* atoms are required for each CH_3OH activation that results in the formation of HCHO or $HCOOCH_3$, which together account for over 88% of the carbon products (Figure 2, 373 K); thus, two is used to approximate the reaction stoichiometries $\nu_{[O^*-*]}$ and $\nu_{[O^*-O^*]}$ in eqs 10a and 10b. $k_{[O^*-*]}$ and $k_{[O^*-O^*]}$ denote the rate constants of CH_3OH activation on O*−* and on O*−O* site pairs, respectively. The atomic ratio of chemisorbed oxygen (O*)-to-unoccupied Pd site (*) during steady-state methanol oxidation catalysis, after rearranging eq 10b, is

$$\frac{[O^*]}{[*]} = \frac{2k_{O_2,f}[O_2]}{\sqrt{(k_{[O^*-*]}[CH_3OH])^2 + 4(k_{O_2,r} + k_{[O^*-O^*]}[CH_3OH])k_{O_2,f}[O_2]} + k_{[O^*-*]}[CH_3OH]} \quad (11)$$

Next, we analyze the relative magnitude of the terms in eq 11, which defines the reversibility of oxygen activation step, because the reversibility is given by the relative rates of oxygen recombination ($r_{O_2,r}$) to methanol conversion ($r_{CH_3OH,[O^*-*]} + r_{CH_3OH,[O^*-O^*]}$). The relative magnitude and reversibility of oxygen activation may differ from one regime to another, as the predominant catalytic route for methanol activation varies.

In regime 1, the rates of oxygen adatom recombination are kinetically insignificant because Pd cluster surfaces are largely uncovered of O* and as such the probability of an O* finding a vicinal O* remains low, making O* recombination followed by molecular desorption an unlikely event. Thus, O* recombination rates must be much lower than the O* reaction rates with CH_3OH, which equal to the net O_2 dissociation rates, and oxygen activation is irreversible in this regime. In regimes 2 and 3, the reversibility of oxygen dissociation steps is inferred from the kinetic dependencies and rates of $^{16}O^{18}O$ isotopologue formation from $^{16}O_2$−$^{18}O_2$ mixtures at the oxygen chemical potential range relevant to methanol oxidation catalysis on surfaces nearly or fully saturated with O* atoms. O* recombination events may be probed from $^{16}O^{18}O$ isotopologue formation with $^{16}O_2$-$^{18}O_2$ mixtures. The rates of $^{16}O^{18}O$ formation on O* covered Pd clusters (2 nm,[36] 8 nm,[36] and 21.3 nm[37] mean cluster diameters) reported previously[36,37] are plotted in Figure 6 as a function of inverse temperature. Extrapolation of these $^{16}O^{18}O$ formation rates from a higher temperature range [1:1 $^{16}O_2$-$^{18}O_2$ mixtures, 2 kPa O_2 at 573−723 K[36] or 0.2−0.6 kPa O_2 at 873 K,[37] activation barrier of 148−152 kJ mol^{-1} on Pd clusters (2 and 8 nm mean cluster diameters)[36]] to 373 K gave $^{16}O^{18}O$ formation rates of 1.4 × 10^{-13} to 7.1 × 10^{-11} mol O_2 (g-atom $Pd_{surface}$-s)$^{-1}$. These O* recombination rates measured at chemical equilibrium are expected to be larger than those during steady-state CH_3OH oxidative dehydrogenation, because CH_3OH scavenges the O* to coverages much lower than equilibrium. In fact, $^{16}O^{18}O$ formation rates in Figure 6 give an estimated rate ratio of oxygen recombination to CH_3OH oxidative dehydrogenation, $r_{^{16}O^{18}O}(r_{ODH,2})^{-1}$ or $r_{^{16}O^{18}O}(r_{ODH,3})^{-1}$, smaller than 10^{-10} over the entire temperature range (313−393 K; e.g. <10^{-11} at 373 K, 0.07−0.20 kPa CH_3OH, 2 kPa O_2), leading us to conclude that

DOI: 10.1021/acscatal.5b00068
ACS Catal. 2015, 5, 3375−3386

O_2 activation must be irreversible at all practical conditions relevant for methanol oxidation catalysis in these regimes.

The much lower rates of O* recombination relative to CH_3OH conversion (Figure 6) and the kinetic evidence of predominant CH_3OH activation on O*−* and O*−O* pairs in regimes 2 and 3, respectively, allow the further simplification of eq 11 [$k_{O_2,r}[O^*]^2 \ll k_{[O^*-*]}[CH_3OH][O^*][*]$ and $k_{O_2,r}[O^*]^2 \ll k_{[O^*-O^*]}[CH_3OH][O^*]^2$ in regimes 2 and 3, respectively] to an expression relating the atomic ratio of oxygen-to-Pd to O_2-to-CH_3OH ratio:

$$\text{regime 2: } \left(\frac{[O^*]}{[*]}\right)_{\text{regime 2}} = \frac{k_{O_2,f}[O_2]}{k_{[O^*-*]}[CH_3OH]} \quad (12a)$$

$$\text{regime 3: } \left(\frac{[O^*]}{[*]}\right)_{\text{regime 3}} = \left(\frac{k_{O_2,f}}{k_{[O^*-O^*]}}\right)^{0.5}\left(\frac{[O_2]}{[CH_3OH]}\right)^{0.5} \quad (12b)$$

These direct relations of [O*]/[*] to O_2-to-CH_3OH ratio or to the square root of O_2-to-CH_3OH ratio via a proportionality constant given by $k_{O_2,f}(k_{[O^*-*]})^{-1}$ in regime 2 or $(k_{O_2,f})^{0.5}(k_{[O^*-O^*]})^{-0.5}$ in regime 3 clearly demonstrate that O* coverages during steady-state methanol oxidative dehydrogenation are prescribed by the O_2-to-CH_3OH ratio. O_2-to-CH_3OH ratio, taken together with the rate constant ratios in eqs 12a and 12b, is a rigorous thermodynamic proxy, as it determines the identity of most abundant surface intermediates, active sites, and kinetically relevant step.

We examine next the CH_3OH pressure and its relation to oxygen coverages required for the kinetic transition from regime 1 to regime 2, defined here to occur at the highest first-order rate coefficient value [38 ± 2 mol (g-atom $Pd_{surface}$-s-kPa)$^{-1}$ in Figure 3, 373 K] attained during methanol oxidative dehydrogenation. The first-order rate coefficients, $k^{1st}_{ODH,i}$ (subscript i denotes regime 1, 2, or 3), and the kinetic transition points on Pd clusters (3.2 nm mean cluster diameter) at 373 K for different methanol pressures (0.75−1.75 kPa) are plotted against the O_2 pressure in Figure 5. These transition points, designated as $[O_2]_t$ (subscript t herein denotes the transition point) and highlighted in Figure 5, occur at the same oxygen coverage [expressed in terms of $([O^*]/[*])_t$], as the identity of most abundant surface intermediates undergoes an incipient transition from mostly uncovered in regime 1 to nearly saturated with O* in regime 2.

$$\left(\frac{[O^*]}{[*]}\right)_t = \left(\frac{k_{O_2,f}}{k_{[O^*-*]}}\right)\left(\frac{[O_2]}{[CH_3OH]}\right)_t \quad (13)$$

As CH_3OH pressure increases, the rates of O* removal by CH_3OH increase proportionally; thus, the oxygen chemical potential at cluster surfaces concomitantly decreases and, as a result, deviates from those at chemical equilibrium. At higher CH_3OH pressures, O_2 pressures required for Pd cluster surfaces to attain the critical O* coverage $([O^*]/[*])_t$ for the transition increase commensurately (e.g., $[O_2]_t$ = 4.8 ± 0.5 kPa for $[CH_3OH]_t$ = 0.75 kPa, $[O_2]_t$ = 11.0 ± 0.5 kPa for $[CH_3OH]_t$ = 1.75 kPa). These effects of CH_3OH reflect a direct, inverse relation of CH_3OH pressure and O* coverages during catalysis. The linear relation for O_2 and CH_3OH pressures to attain the critical O* coverage for the transition from regime 1 to regime 2 {$[O_2]_t$ and $[CH_3OH]_t$, respectively} for 2.5, 3.2, and 7.7 nm Pd clusters at 373 K is captured in Figure 7, and the catalytic effects of cluster diameter are discussed in section 3.5. The

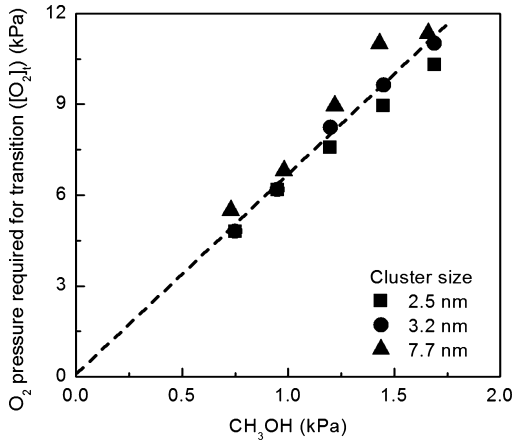

Figure 7. Oxygen pressures required for kinetic transition between regimes 1 and 2, $[O_2]_t$, plotted as a function of methanol pressure, during CH_3OH oxidative dehydrogenation at 373 K on Pd clusters (2.5 nm (■), 3.2 nm (●), and 7.7 nm (▲) mean Pd cluster diameter) (0.5 (■) and 1.0 (●, ▲) wt % Pd/SiO_2, 200 SiO_2-to-catalyst intraparticle and 5700 SiO_2-to-catalyst interparticle dilution ratios; 1.26×10^8 cm^3 g_{cat}^{-1} h^{-1}).

slope of this relation, which corresponds to an oxygen-to-methanol ratio of 7 ± 1, reflects the operating boundary for regimes 1 and 2, irrespective of cluster sizes (2.5−7.7 nm). The O* coverage ([O*]/[L] = 0.55 ± 0.05, estimated from eq S6 in section S2 of the Supporting Information) at these kinetic transition points equals those at chemical equilibrium with O_2, attained in the limit of zero CH_3OH pressure.

3.4. Temperature Effects on the Transition among Regimes and Their Associated Kinetic Parameters for Methanol Oxidative Dehydrogenation. We explore next the effects of temperature on the operating boundary between the regimes and their respective rate constant values. First-order rate coefficients ($k^{1st}_{ODH,i}$) for methanol oxidative dehydrogenation on Pd clusters (1.0 wt % Pd/SiO_2, 3.2 nm mean Pd cluster diameter) at different temperatures (323−393 K) were determined by varying the CH_3OH and O_2 pressures independently over pressure ranges (0.5−2.0 kPa CH_3OH, 0.1−60 kPa O_2) corresponding to O_2-to-CH_3OH ratios between 0.1 to 30. These rate coefficient values, irrespective of the individual reactant pressures and temperature, exhibit similar single-valued functional dependencies with the O_2-to-CH_3OH ratio, as shown in Figure 8a, because the operating kinetic regimes, their associated kinetically relevant step, and the identity of most abundant surface intermediates remain the same as those described in section 3.2. As the temperature increases, transitions from one regime to another occur at higher O_2-to-CH_3OH ratios (e.g., 2.6 ± 0.4 at 323 K and 14 ± 1 at 393 K). These transitions all occur at a critical oxygen coverage, expressed in terms of $([O^*]/[*])_t$, at which the identity of the most abundant surface intermediates converts from *−* to O*−* pairs. The O_2-to-CH_3OH ratio required to attain the critical oxygen coverage $([O^*]/[*])_t$ for the transition from regime 1 to 2, $([O_2][CH_3OH]^{-1})_t$, depends on the rate constant ratio of methanol activation to oxygen dissociation [derived from eq 13] and thus on temperature, after expressing the rate constants for methanol activation

DOI: 10.1021/acscatal.5b00068
ACS Catal. 2015, 5, 3375−3386

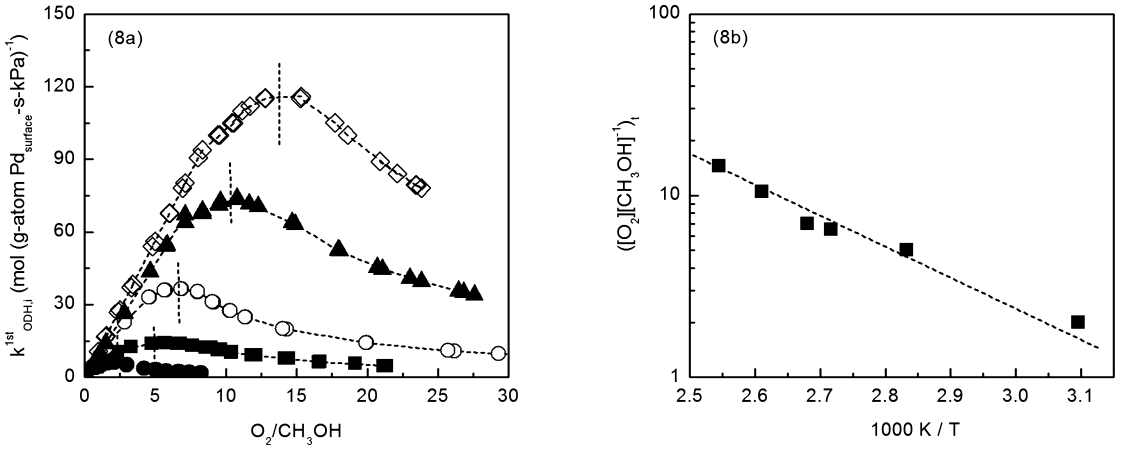

Figure 8. (a) First-order rate coefficients ($k^{1st}_{ODH,i} = r_{ODH,i}[CH_3OH]^{-1}$, subscript i denotes regime i (i = 1, 2, or 3)) for CH_3OH oxidative dehydrogenation (ODH) as single-valued functions of O_2-to-CH_3OH ratio during CH_3OH–O_2 reactions (0.5–2.0 kPa CH_3OH, 0.1–60 kPa O_2) on Pd clusters at 323 K (●), 353 K (■), 373 K (○), 383 K (▲), and 393 K (◊). (b) Measured O_2-to-CH_3OH ratios required for transition between regimes 1 and 2, $([O_2][CH_3OH]^{-1})_t$, during methanol oxidation on Pd clusters as a function of inverse temperature (1.0 wt % Pd/SiO_2, 3.2 nm mean Pd cluster diameter, 200 SiO_2-to-catalyst intraparticle and 5700 SiO_2-to-catalyst interparticle dilution ratios; 1.26 × 10^8 cm^3 g_{cat}^{-1} h^{-1}).

($k_{[O^*-*]}$) and oxygen dissociation ($k_{O_2,f}$) in an Arrhenius form of

$$\left(\frac{[O_2]}{[CH_3OH]}\right)_t = \frac{k_{[O^*-*]}}{k_{O_2,f}}\left(\frac{[O^*]}{[*]}\right)_t = \frac{A_{[O^*-*]}}{A_{O_2,f}} \exp\left[-\frac{(E_{A,[O^*-*]} - E_{A,O_2,f})}{RT}\right]\left(\frac{[O^*]}{[*]}\right)_t \quad (14)$$

$$\ln\left(\frac{[O_2]}{[CH_3OH]}\right)_t = \ln\left(\frac{[O^*]}{[*]}\right)_t + \ln\left(\frac{A_{[O^*-*]}}{A_{O_2,f}}\right) - \frac{1}{RT}(E_{A,[O^*-*]} - E_{A,O_2,f}) \quad (15)$$

$A_{[O^*-*]}$ and $A_{O_2,f}$ are the pre-exponential factors and $E_{A,[O^*-*]}$ and $E_{A,O_2,f}$ are the activation barriers for methanol activation on an O*–* pair and oxygen dissociation, respectively. The correlation in eq 15 relates the oxygen-to-methanol ratio required for the transition between regime 1 and 2, $([O_2][CH_3OH]^{-1})_t$, to inverse temperature, as captured in Figure 8b. The slope of this line, $-(E_{A,[O^*-*]} - E_{A,O_2,f})R^{-1}$, is the difference in activation barrier for methanol activation and oxygen dissociation divided by gas constant R.

Rate constants $k_{O_2,f}$, $k_{[O^*-*]}$, and $k_{[O^*-O^*]}$ are derived from regression of the rate data in Figure 8a with the respective rate equation (eqs 3, 5, and 7 for regimes 1, 2, and 3, respectively) and shown in Figure 9 as a function of inverse temperature, whereas the associated barriers and pre-exponential values are summarized in Table 2. The activation barrier for oxygen dissociation on largely uncovered Pd clusters (regime 1), $E_{A,O_2,f}$, is 24 ± 5 kJ $(mol\ O_2)^{-1}$. This step at low coverages is expected to occur readily with no barrier, as calculated by density functional studies on Pd(111), Pd(100), and Pd(110) surfaces.[38] The observed activated nature of this step may reflect an increase in the total Pd sites available for CH_3OH oxidation catalysis with increasing temperature. A small portion of Pd sites, specifically the coordinative unsaturated sites at corners and edges, may bind to methanol derived species

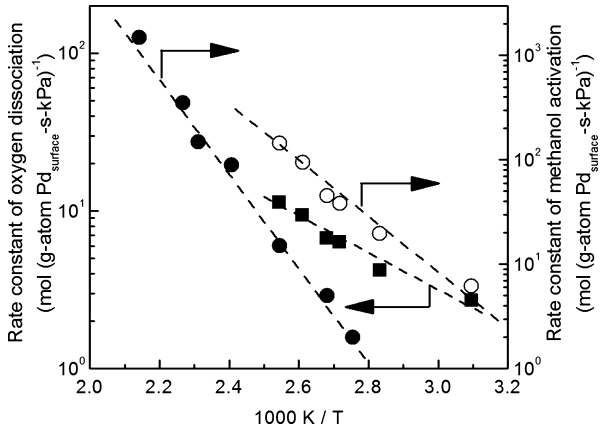

Figure 9. Rate constants of oxygen dissociation ($k_{O_2,f}$, ■) on uncovered Pd cluster surfaces, of methanol activation on O*–* site pair ($k_{[O^*-*]}$, ○), and of methanol activation on O*–O* site pair ($k_{[O^*-O^*]}$, ●) during CH_3OH–O_2 reactions on Pd clusters as a function of inverse temperature (1.0 wt % Pd/SiO_2, 3.2 nm mean Pd cluster diameter, 200 SiO_2-to-catalyst intraparticle and 5700 SiO_2-to-catalyst interparticle dilution ratios; 323–473 K; 1.26 × 10^8 cm^3 g_{cat}^{-1} h^{-1}).

during catalysis. As an example, CH_3O* adsorption energies are −184 kJ mol^{-1} on the edge site and −138 kJ mol^{-1} on the terrace site of a truncated-octahedral cluster with 79 Pd atoms.[39] CO* adsorption energies are −188 kJ mol^{-1} on the edge site of an octahedral cluster with 146 Pd atoms and −142 kJ mol^{-1} on the terrace site of a cuboctahedral cluster with 147 Pd atoms.[40] It is plausible that these intermediates remain bound to a small fraction of Pd sites, especially those with lower coordination, at coverages that remain unchanged with pressures because of their stronger bindings, causing them to remain occupied and unable to participate in catalytic turnovers at low temperatures. At higher temperature, the binding species desorb and, as a result, these sites become catalytically active. This effect of temperature on the catalytic participation of low coordination Pd atoms may lead to the low barrier [24 ± 5 kJ $(mol\ O_2)^{-1}$] measured for O_2 dissociation.

The effective rate constant for regime 2 [$k_{eff,2} = k_{[O^*-*]}^2 k_{O_2,f}^{-1}$, eq 6] contains the elementary rate constants

DOI: 10.1021/acscatal.5b00068
ACS Catal. 2015, 5, 3375–3386

Table 2. Measured Activation Barriers and Entropies for Methanol Oxidative Dehydrogenation on Pd Clusters in Kinetic Regimes 1−3[a]

kinetic regime i	active sites	effective barrier ($E_{A,eff,i}$) (kJ mol^{-1})	pre-exponential factor ($A_{eff,i}$) (kPa^{-1} s^{-1})	activation barrier for O_2 dissociation ($E_{A,n}$) (kJ mol^{-1})	activation barrier for CH_3OH activation ($E_{A,n}$) (kJ mol^{-1})	activation entropy ($\Delta S^{\ddagger}_n$) (J mol^{-1} K^{-1})
regime 1	*−*	26 ± 5	3×10^4	24 ± 5	NA[b]	−185 ± 10
regime 2	O*−*	83 ± 3	1.4×10^{14}	24 ± 5	53 ± 5	−97 ± 10[a]
regime 3	O*−O*	90 ± 3	1.9×10^{13}	NA	90 ± 3	−18 ± 10

[a]Activation entropy for methanol activation on O*−* site pair; the subscript i in effective barrier ($E_{A,eff,i}$) and pre-exponential factor ($A_{eff,i}$) denotes regime i (i = 1, 2, or 3); the subscript n in activation barrier ($E_{A,n}$) and activation entropy ($\Delta S^{\ddagger}_n$) denotes O_2 dissociation, CH_3OH activation on O*−* site pair or on O*−O* site pair (n = (O_2,f), [O*−*], or [O*−O*]); 1.0 wt % Pd/SiO_2, 3.2 nm mean Pd cluster diameter, 200 SiO_2-to-catalyst intraparticle and 5700 SiO_2-to-catalyst interparticle dilution ratios; 323−473 K; 1.26×10^8 cm^3 g_{cat}^{-1} h^{-1}. [b]NA = not applicable.

for CH_3OH activation on O*−* site pair ($k_{[O*-*]}$) and O_2 dissociation ($k_{O_2,f}$). The CH_3OH activation step cleaves the CH_3O--H bond, as proposed previously on the basis of temperature-programmed decomposition of CH_3OH on O*-covered Pd(100),[41] Pd(111),[42] Ag(110),[27] and Pt(111)[28] surfaces, temperature-programmed desorption of CH_3CHO from C_2H_5OH reactions with preadsorbed O* on Au(111) surfaces,[18] and density functional theory calculations[11,12,14−16] of CH_3OH dissociation on oxygen-covered single-crystal surfaces [1/9 ML O*/Au(111),[11,12] 0.25 ML O*/Cu(110),[14] and 0.5 ML O*/Ir(111)[15]] and RuO_2(110) surfaces.[16] The rate constants $k_{[O*-*]}$ are decoupled from those of O_2 dissociation ($k_{O_2,f}$) by assuming that the rate constants and barriers for the O_2 dissociation step are independent of O* coverages and thus remain the same across regimes 1 and 2. This is an approximation because the barriers are expected to be higher on O*-covered surfaces (regime 2) as a result of the lower heat of O* adsorption than on uncovered surfaces (regime 1), according to the prediction from Brønsted−Evans−Polanyi relation between the barrier and the heat of reaction (also the heat of O* adsorption).[43,44] The decrease in the heat of O* adsorption with coverages was verified on Pd(111) surfaces based on calorimetric measurement[35] and the relation of heat of O* adsorption and O_2 dissociation barrier was confirmed from density functional theory calculations on Pt(111) surfaces.[45] The rate constant value gives an estimated barrier ($E_{A,[O*-*]}$) and activation entropy ($\Delta S^{\ddagger}_{[O*-*]}$) of 53 ± 5 kJ mol^{-1} and −97 ± 10 J mol^{-1} K^{-1}, respectively, for CH_3OH activation on O*−* pairs (in regime 2). The barriers are much lower than those for methanol activation on *−* pairs, determined from density functional theory calculations on Pd(111) to be 100 kJ mol^{-1},[46,47] because the O* in the O*−* pair acts as a Brønsted base that abstracts the H from the O−H bond. The catalytic involvement of O* on promoting the O−H cleavage and thus lowering the CH_3OH activation barriers is general, as previously found for the case on Au(111) (activation barrier of 21 kJ mol^{-1} on O*−* vs 180 kJ mol^{-1} on *−*)[12] and Cu(110) (activation barrier of 33 kJ mol^{-1} on O*−* vs 100 kJ mol^{-1} on *−*)[14] surfaces. DFT studies shows O* (denoted as O^{I}*) atom stabilizing the CH_3O^{II}—H activation transition state, $(CH_3O^{II}—H—O^{I}*)^{\ddagger}$, on Au(111) surfaces by forming a nearly fully formed O^{I}−H bond with the leaving H (O^{I}−H bond distance of 1.19 Å at transition state vs 1.03 Å at product state) whereas the O^{II}—H bond remains largely intact at 1.26 Å (compare with the O^{II}−H of 0.98 Å in the reactant state) and the CH_3O^{II} interact strongly with a vicinal Au atom (O^{II}−Au bond distance of 2.26 Å at transition state vs 2.09 Å at product state where CH_3O^{II} adsorbed on Au atom through its O^{II} atom).[12] In contrast, CH_3OH activation on *−* pairs in the absence of O* occurs via a nearly fully formed CH_3O^{II}--* bond (O^{II}−Au bond distance of 2.14 Å at transition state vs 2.04 Å at the product state) at much higher barriers (180 kJ mol^{-1} on *−* vs 21 kJ mol^{-1} on O*−*).[12] Comparing with the opposite case of CH_3OH activation on O* saturated surfaces, on which Pd atoms are occupied by O* and remain inaccessible to CH_3OH (regime 3), the barrier on O*−* pairs is lower and the activation entropy losses are higher (more negative) than on O*−O* pairs [$E_{A,[O*-*]}$ = 53 ± 5 kJ mol^{-1} and $\Delta S^{\ddagger}_{[O*-*]}$ = −97 ± 10 J mol^{-1} K^{-1} on O*−* pairs (regime 2) versus $E_{A,[O*-O*]}$ = 90 ± 3 kJ mol^{-1} and $\Delta S^{\ddagger}_{[O*-O*]}$ = −18 ± 10 J mol^{-1} K^{-1} on O*−O* pairs (regime 3)]. The lower barriers and larger entropy losses in regime 2 reflect the involvement of exposed Pd atoms as "landing sites" that interact with CH_3O fragments at the transition states more strongly than for the case of O*−O* pairs.

3.5. Effects of Pd Cluster Diameter on Methanol Oxidative Dehydrogenation Rates. As Pd clusters become larger, the fraction of Pd atoms located at the coordinative unsaturated corners and edges decreases but those at crystal facets concomitantly increase,[48] and as a result, the average coordination of surface Pd increases. For example, the average coordination numbers are 6.75 and 8.60 for exposed metal sites on 1.0 and 7.9 nm cuboctahedral clusters with face-centered cubic unit cell structures, respectively, predicted based on the theoretical model by Van Hardeveld and Hartog,[48] considering the statistical distributions of the various types of sites (edges, corner, closed packed (111) and (100) surfaces). The average coordination number approaches 9.00 on ideal (111) surfaces; as the average coordination number increases with cluster diameter, the average binding strength of chemisorbed oxygen concomitantly decreases.[2,37] These effects of coordinative unsaturation on the rate and thermodynamic constants and the resulting methanol turnover rates are probed by varying the average Pd cluster diameter in 0.5 and 1.0 wt % Pd/SiO_2 catalysts from 2.5, 3.2, to 7.7 nm (average coordination numbers are 8.11, 8.27, and 8.59 for 2.5, 3.2, and 7.7 nm Pd clusters, respectively) at 373 K and the first-order rate coefficients for these samples are shown as a function of O_2-to-CH_3OH ratio in Figure 10. These rate coefficients exhibit identical dependencies with O_2-to-CH_3OH ratios, but their values were higher on the larger than the smaller clusters.

The rate coefficients ($k_{eff,1}$, $k_{eff,2}$, and $k_{eff,3}$) for all regimes and the rate constant ratio ($k_{[O*-*]}k_{O_2,f}^{-1}$) for regime 2, extracted from the rate data in Figure 10, are shown in Figure 11 as a function of cluster diameter (2.5−7.7 nm). The effective rate constant ($k_{eff,1}$) in regime 1, which also equals the O_2 dissociation rate constant ($k_{O_2,f}$), increases by a factor of 2.2 ± 0.2 as cluster diameter increases from 2.5 to 7.7 nm. The O_2 dissociation step exhibits a low activation barrier [24 kJ (mol O_2)$^{-1}$ on 3.2 nm Pd clusters, Table 2] which does not vary

DOI: 10.1021/acscatal.5b00068
ACS Catal. 2015, 5, 3375−3386

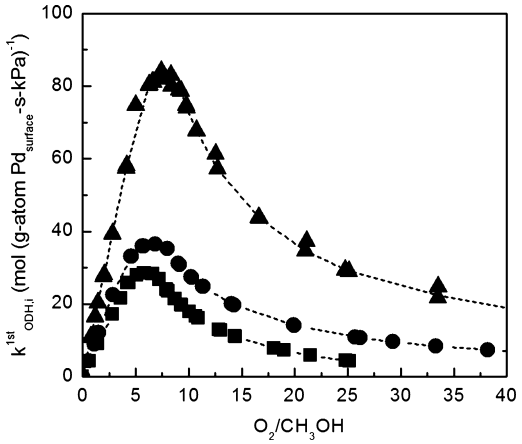

Figure 10. First-order rate coefficients ($k^{1st}_{ODH,i} = r_{ODH,i}\,[CH_3OH]^{-1}$, subscript i denotes regime i (i = 1, 2, or 3)) for CH_3OH oxidative dehydrogenation (ODH) at 373 K on supported Pd clusters of different mean diameters (2.5 nm (■), 3.2 nm (●), and 7.7 nm (▲)) as a function of O_2-to-CH_3OH ratio (0.5 (■) and 1.0 (●, ▲) wt % Pd/SiO_2, 200 SiO_2-to-catalyst intraparticle and 5700 SiO_2-to-catalyst interparticle dilution ratios; 1.26×10^8 cm^3 g_{cat}^{-1} h^{-1}).

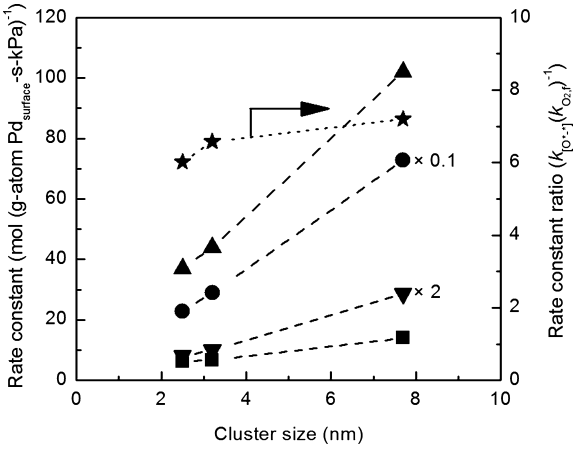

Figure 11. Cluster size dependence of rate constants for O_2 dissociation ($k_{O_2,f}$, ■), CH_3OH activation on O*−* site pair ($k_{[O^*-*]}$, ▲), and CH_3OH activation on O*−O* site pair ($k_{[O^*-O^*]}$, ▼), effective rate constant in regime 2 ($k_{eff,2}=k_{[O^*-*]}{}^2k_{O_2,f}{}^{-1}$, ●), and rate constant ratio of CH_3OH activation to O_2 dissociation ($k_{[O^*-*]}(k_{O_2,f})^{-1}$, ★) on Pd clusters at 373 K (0.5 (2.5 nm Pd clusters) and 1.0 (3.2 and 7.7 nm Pd clusters) wt % Pd/SiO_2, 200 SiO_2-to-catalyst intraparticle and 5700 SiO_2-to-catalyst interparticle dilution ratios; 1.26×10^8 cm^3 g_{cat}^{-1} h^{-1}).

markedly with the heat of oxygen adsorption ($O_2 + 2* \rightarrow 2O*$, $\Delta H_{O_2} = -205$ kJ (mol O_2)$^{-1}$ at 300 K on bare Pd(111) surfaces[35]); thus, the rate constant is expected to remain insensitive to cluster diameter. The cluster size effects on rate constant may be caused by a small amount of reactive intermediates (e.g., CH_3O* and/or CO*) that preferentially bind to coordinatively unsaturated corner and edge sites and more strongly on smaller than larger clusters at coverages independent of pressures. As a result of site occupation insensitive to pressure variation, these sites remain kinetically silent. In fact, the heats of adsorption for CH_3O* and CO* vary strongly with the adsorption sites: CH_3O* adsorption energies on a Pd cluster are −184 kJ mol^{-1} on edge sites versus −138 kJ mol^{-1} on terrace sites,[39] and those for CO* adsorption on the same sites are −188 kJ mol^{-1} versus −144 kJ mol^{-1}, respectively.[40] On the larger clusters, the fraction of coordinatively unsaturated corner and edge remains insignificant; thus, all sites participate in catalysis.

The effective rate constants ($k_{eff,2}=k_{[O^*-*]}{}^2k_{O_2,f}{}^{-1}$) in regime 2 increase with increasing cluster diameter (Figure 11). The elementary rate constants for CH_3OH activation on O*−* site pair ($k_{[O^*-*]}$), are decoupled from the effective rate constants by assuming the O_2 dissociation rate constants ($k_{O_2,f}$) remained insensitive to O* coverages. The rate constants for CH_3OH activation on O*−* sites increase to the similar extents with that of O_2 dissociation (by 2.7 ± 0.1 times as cluster size increases from 2.5 to 7.7 nm). These effects of cluster size on the rate constants lead to an increase in the effective rate constant ($k_{eff,2} = k_{[O^*-*]}{}^2k_{O_2,f}{}^{-1}$) by a factor of 3.2 ± 0.2. The rate constants for CH_3OH activation on O*−* site pair ($k_{[O^*-*]}$) depend on the free energies for a $CH_3OH(g)$ to evolve a $(CH_3O*\text{--}H\text{--}O*)^{\ddagger}$ transition state and the extent of interactions between CH_3O with a Pd atom, the O* and the leaving H atom, and the O and the leaving H atom in CH_3OH. An increase in the coordination of surface Pd atoms weaken their bindings to CH_3O*, and to the O* atoms, and in turn, strengthens the bindings of O* to the leaving H atom. These concomitant effects of weaker CH_3O* bindings and stronger H bindings to O* appear to compensate one another, leading to the structure sensitivity effects.

The rate constant for CH_3OH activation on O*−O* sites pair ($k_{[O^*-O^*]}$), which equals the first-order rate coefficient in regime 3 ($k^{1st}_{ODH,3} = r_{ODH,3}\,[CH_3OH]^{-1}$), increases with increasing cluster size (Figure 11). The weakly bound O* atoms prevalent on the larger clusters are more basic and thus more effective in electron donation to the leaving H during the O−H bond activation in CH_3OH, as reflected from an increase in the rate constant for CH_3OH activation by a proportionally factor of 3.4 ± 0.2 for the larger than the smaller Pd clusters (7.7 nm vs 2.5 nm). Similar effects of O* binding energies on their reactivity toward methanol activation on O*−O* sites pair were observed when comparing metals with different O* binding strengths: larger CH_3OH activation rate constants were measured for Pt than Pd, as Pt binds O* more weakly (rate constant of 251 vs 5 mol CH_3OH (g-atom $Pd_{surface}$-s-kPa)$^{-1}$ at 373 K[20] and O* binding energies of −354 kJ mol^{-1} vs −382 kJ mol^{-1} for Pt vs Pd,[49] respectively).

4. CONCLUSION

Complex kinetic dependencies and their underlying mechanistic interpretation for methanol oxidative dehydrogenation on dispersed Pd clusters are established on the basis of rate measurements in the kinetically controlled regime and oxygen uptake studies. Three kinetic regimes, each with a unique dependence for methanol oxidative dehydrogenation and for products formation, are resulted from a dynamic transition in oxygen coverages and the concomitant transition in the kinetically relevant step in response to changing the oxygen-to-methanol ratio because this ratio is a rigorous thermodynamic proxy of oxygen chemical potential at Pd cluster surfaces during methanol oxidation catalysis. As oxygen coverages increase from uncovered to saturation, the identity of the kinetically relevant step varies from oxygen dissociation on Pd atom pairs, to CH_3OH activation on oxygen adatom and oxygen vacancy pairs, and then to CH_3OH activation on

DOI: 10.1021/acscatal.5b00068
ACS Catal. 2015, 5, 3375−3386

oxygen adatom pairs. The direct relation of oxygen coverages and O_2-to-CH_3OH ratios and their influences on the identity of kinetically relevant step lead to a generalized, single-valued functional correlation between first-order rate coefficients and O_2-to-CH_3OH ratios. CH_3OH activation on oxygen adatom and oxygen vacancy pairs exhibits lower activation barriers and higher entropy losses than on oxygen adatom pairs, because oxygen vacancies provide the "landing sites" that interact more strongly with the CH_3O fragment at the transition state. In all regimes, methanol turnover rates increase with cluster diameter because of (i) an increase in the availability of unoccupied Pd sites for O_2 dissociation in regime 1 and (ii) a decrease in oxygen binding strengths and therefore a concomitant increase in oxygen reactivities in regimes 2 and 3. These effects of surface coverages and cluster sizes, when recognized, reduce the apparent complex kinetic phenomena into a simple correlation of rate coefficients and the operating O_2-to-CH_3OH ratios. Such a relation reflects the defining roles of the thermodynamic activities of surface oxygen on their reactivities for oxidation catalysis and appears to be general across other classes of oxidation reactions.

■ ASSOCIATED CONTENT

Supporting Information

The following file is available free of charge on the ACS Publications website at DOI: 10.1021/acscatal.5b00068.

Additional derviation information (PDF)

■ AUTHOR INFORMATION

Corresponding Author

*E-mail: cathy.chin@utoronto.ca. Homepage: http://www.labs.chem-eng.utoronto.ca/catalysis/.

Notes

The authors declare no competing financial interest.

■ ACKNOWLEDGMENTS

This study was supported by Natural Sciences and Engineering Research Council of Canada and Canada Foundation for Innovation.

■ REFERENCES

(1) Wittstock, A.; Zielasek, V.; Biener, J.; Friend, C.; Bäumer, M. *Science* **2010**, *327*, 319−322.
(2) Tu, W.; Chin, Y.-H. *J. Catal.* **2014**, *313*, 55−69.
(3) Lichtenberger, J.; Lee, D.; Iglesia, E. *Phys. Chem. Chem. Phys.* **2007**, *9*, 4902−4906.
(4) Jørgensen, B.; Egholm Christiansen, S.; Dahl Thomsen, M. L.; Christensen, C. H. *J. Catal.* **2007**, *251*, 332−337.
(5) Takei, T.; Iguchi, N.; Haruta, M. *New J. Chem.* **2011**, *35*, 2227−2233.
(6) Biella, S.; Rossi, M. *Chem. Commun.* **2003**, 378−379.
(7) Santasalo-Aarnio, A.; Kwon, Y.; Ahlberg, E.; Kontturi, K.; Kallio, T.; Koper, M. T. M. *Electrochem. Commun.* **2011**, *13*, 466−469.
(8) Zhao, H.; Bennici, S.; Shen, J.; Auroux, A. *J. Mol. Catal. A: Chem.* **2009**, *309*, 28−34.
(9) Liu, H.; Iglesia, E. *J. Phys. Chem. B* **2005**, *109*, 2155−2163.
(10) Soares, A. P. V.; Portela, M. F.; Kiennemann, A. *Catal. Rev.: Sci. Eng.* **2005**, *47*, 125−174.
(11) Xu, B.; Haubrich, J.; Baker, T. A.; Kaxiras, E.; Friend, C. M. *J. Phys. Chem. C* **2011**, *115*, 3703−3708.
(12) Liu, S.; Jin, P.; Zhang, D.; Hao, C.; Yang, X. *Appl. Surf. Sci.* **2013**, *265*, 443−451.
(13) Lausche, A. C.; Hummelshøj, J. S.; Abild-Pedersen, F.; Studt, F.; Nørskov, J. K. *J. Catal.* **2012**, *291*, 133−137.
(14) Sakong, S.; Gross, A. *J. Phys. Chem. A* **2007**, *111*, 8814−8822.
(15) Wang, H.; He, C.-z.; Huai, L.-y.; Liu, J.-y. *J. Phys. Chem. C* **2013**, *117*, 4574−4584.
(16) Lopez, N.; Novell-Leruth, G. *Phys. Chem. Chem. Phys.* **2010**, *12*, 12217−12222.
(17) Petitjean, H.; Tarasov, K.; Delbecq, F. o.; Sautet, P.; Krafft, J. M.; Bazin, P.; Paganini, M. C.; Giamello, E.; Che, M.; Lauron-Pernot, H. l. n.; Costentin, G. n. *J. Phys. Chem. C* **2010**, *114*, 3008−3016.
(18) Gong, J.; Mullins, C. B. *J. Am. Chem. Soc.* **2008**, *130*, 16458−16459.
(19) Gong, J.; Flaherty, D. W.; Yan, T.; Mullins, C. B. *ChemPhysChem* **2008**, *9*, 2461−2466.
(20) Tu, W.; Chin, Y.-H. *Angew. Chem., Int. Ed.* **2014**, *53*, 12148−12152.
(21) Chin, Y. H.; Buda, C.; Neurock, M.; Iglesia, E. *J. Catal.* **2011**, *283*, 10−24.
(22) Chin, Y.-H.; Buda, C.; Neurock, M.; Iglesia, E. *J. Am. Chem. Soc.* **2011**, *133*, 15958−15978.
(23) García-Diéguez, M.; Chin, Y.-H.; Iglesia, E. *J. Catal.* **2012**, *285*, 260−272.
(24) Lide, D. R. *Handbook of Chemistry and Physics*, 87th ed.; CRC Press: Boca Raton, FL, 2006.
(25) McCabe, R. W.; Mitchell, P. J. *J. Catal.* **1987**, *103*, 419−425.
(26) McCabe, R.; Mitchell, P. *Appl. Catal.* **1986**, *27*, 83−98.
(27) Wachs, I. E.; Madix, R. J. *Surf. Sci.* **1978**, *76*, 531−558.
(28) Akhter, S.; White, J. M. *Surf. Sci.* **1986**, *167*, 101−126.
(29) Kizhakevariam, N.; Stuve, E. M. *Surf. Sci.* **1993**, *286*, 246−260.
(30) Savara, A.; Chan-Thaw, C. E.; Rossetti, I.; Villa, A.; Prati, L. *ChemCatChem* **2014**, *6*, 3464−3473.
(31) Ishikawa, A.; Neurock, M.; Iglesia, E. *J. Am. Chem. Soc.* **2007**, *129*, 13201−13212.
(32) Chin, Y.-H.; Buda, C.; Neurock, M.; Iglesia, E. *J. Am. Chem. Soc.* **2013**, *135*, 15425−15442.
(33) Atkins, P. W. *Physical Chemistry*, 6th ed.; Oxford University Press: New York, 1998; pp 97−124.
(34) Peter, M.; Adamovsky, S.; Flores Camacho, J. M.; Schauermann, S. *Faraday Discuss.* **2013**, *162*, 341−354.
(35) Peter, M.; Flores Camacho, J. M.; Adamovski, S.; Ono, L. K.; Dostert, K.-H.; O'Brien, C. P.; Roldan Cuenya, B.; Schauermann, S.; Freund, H.-J. *Angew. Chem., Int. Ed.* **2013**, *52*, 5175−5179.
(36) Weiss, B. M.; Iglesia, E. *J. Catal.* **2010**, *272*, 74−81.
(37) Chin, Y.-H.; Iglesia, E. *J. Phys. Chem. C* **2011**, *115*, 17845−17855.
(38) Wang, Z.; Jia, X.; Wang, R. *J. Phys. Chem. A* **2004**, *108*, 5424−5430.
(39) Kozlov, S. M.; Cabeza, G. F.; Neyman, K. M. *Chem. Phys. Lett.* **2011**, *506*, 92−97.
(40) Yudanov, I. V.; Sahnoun, R.; Neyman, K. M.; Rösch, N.; Hoffmann, J.; Schauermann, S.; Johanek, V.; Unterhalt, H.; Rupprechter, G.; Libuda, J. *J. Phys. Chem. B* **2003**, *107*, 255−264.
(41) Jorgensen, S. W.; Madix, R. *Surf. Sci.* **1987**, *183*, 27−43.
(42) Davis, J.; Barteau, M. *Surf. Sci.* **1988**, *197*, 123−152.
(43) van Santen, R. A.; Neurock, M.; Shetty, S. G. *Chem. Rev.* **2009**, *110*, 2005−2048.
(44) Nørskov, J. K.; Bligaard, T.; Hvolbæk, B.; Abild-Pedersen, F.; Chorkendorff, I.; Christensen, C. H. *Chem. Soc. Rev.* **2008**, *37*, 2163−2171.
(45) Allian, A. D.; Takanabe, K.; Fujdala, K. L.; Hao, X.; Truex, T. J.; Cai, J.; Buda, C.; Neurock, M.; Iglesia, E. *J. Am. Chem. Soc.* **2011**, *133*, 4498−4517.
(46) Schennach, R.; Eichler, A.; Rendulic, K. D. *J. Phys. Chem. B* **2003**, *107*, 2552−2558.
(47) Jiang, R.; Guo, W.; Li, M.; Fu, D.; Shan, H. *J. Phys. Chem. C* **2009**, *113*, 4188−4197.
(48) Van Hardeveld, R.; Hartog, F. *Surf. Sci.* **1969**, *15*, 189−230.
(49) van Santen, R. A.; Neurock, M. *Molecular heterogeneous catalysis: a conceptual and computational approach*. John Wiley & Sons: Weinheim, 2006; p 105−112.

DOI: 10.1021/acscatal.5b00068
ACS Catal. 2015, 5, 3375−3386